ACCSCIENCE PUBLISHING

International Journal of Bioprinting

RESEARCH ARTICLE

A quantitative calibration strategy for reproducible extrusion-based bioprinting using gelatin methacryloyl hydrogels

Laura Mendoza-Cerezo[1,2], Jesús M. Rodríguez-Rego[1*], Antonio Macías-García[3], Silvia M. Díaz-Prado[4,5], and Alfonso C. Marcos-Romero[1*]

[1]Department of Graphic Expression, School of Industrial Engineering, University of Extremadura, Badajoz, Spain

[2]Department of Biochemistry, Faculty of Sciences, University of Extremadura, Badajoz, Spain

[3]Department of Mechanical, Energy and Materials Engineering, School of Industrial Engineering, University of Extremadura, Badajoz, Spain

[4]Cell Therapy and Regenerative Medicine Research Group, Galician Public Foundation for Biomedical Research (INIBIC), Faculty of Health Sciences, Center for Advanced Scientific Research (CICA), University of A Coruña, 15006 A Coruña, Spain.

[5]Biomedical Research Networking Center in Bioengineering, Biomaterials and Nanomedicine (CIBER-BBN), 28029 Madrid, Spain.

***Corresponding authors:**
Jesús M. Rodríguez-Rego (jesusrodriguezrego@unex.es)

Alfonso C. Marcos-Romero (acmarcos@unex.es)

Citation: Mendoza-Cerezo L, Rodríguez-Rego J, Macías-García A, Díaz-Prado S, Marcos-Romero A. A quantitative calibration strategy for reproducible extrusion-based bioprinting using gelatin methacryloyl hydrogels. *Int J Bioprint*. 2026:12(2):025480500. doi: 10.36922/IJB025480500

Received: November 29, 2025
1st revised: January 2, 2026
2nd revised: January 11, 2026
Accepted: January 19, 2026
Published Online: January 19, 2026

Copyright: © 2026 Author(s). This is an Open Access article distributed under the terms of the Creative Commons Attribution License, permitting distribution, and reproduction in any medium, provided the original work is properly cited.

Publisher's Note: AccScience Publishing remains neutral with regard to jurisdictional claims in published maps and institutional affiliations.

Abstract

Extrusion-based three-dimensional bioprinting remains limited by the absence of standardized methods to define the pressure conditions required for stable hydrogel flow. As a result, most workflows still rely on empirical tuning, which compromises reproducibility, structural fidelity, and interlaboratory comparability. Addressing this gap requires quantitative tools capable of identifying the minimum pressure for extrusion and the pressure range in which continuous, defect-free flow is maintained. This work presents a modular characterization platform integrating real-time pressure sensing, together with nozzle temperature regulation and environmental monitoring (temperature, humidity, and carbon dioxide) to ensure controlled and reproducible extrusion conditions. Using 10% gelatin methacryloyl, force–displacement curves revealed a stabilization pressure of 165 kPa, associated with continuous extrusion and minimal geometric deviation, and bounded by experimentally validated under-extrusion (155 kPa) and over-extrusion (185 kPa) conditions. Bioprinting tests confirmed that operating within this stabilization zone improves filament uniformity, print fidelity, and dimensional accuracy compared with under- and over-extrusion regimes. Quantitative metrics, including deflection analysis, printability parameter, void–area similarity, and structural similarity index, demonstrated superior reproducibility at the stabilization pressure. Biological validation using MCF-7 cells showed that 165 kPa preserved high viability (97.9%), whereas extrusion at 185 kPa reduced survival to 88.6%, confirming the sensitivity of cell integrity to excess shear stress. Together, these findings establish a sensor-driven calibration strategy that replaces trial-and-error parameter selection with quantitative and reproducible pre-print optimization. The device is compatible with commercial bioprinters and provides a practical framework for improving process standardization, structural fidelity, and biological safety in extrusion-based bioprinting. The platform is conceived as an independent, modular device for experimental calibration of extrusion parameters prior to bioprinting.

Keywords: Cell viability; Cytotoxicity; Modular characterization device; Three-dimensional bioprinting; Three-dimensional design; Tissue engineering

1. Introduction

Extrusion-based three-dimensional (3D) bioprinting is a central technique in tissue engineering due to its capacity to fabricate cell-laden structures with controlled architectures and clinically relevant geometries.[1–3] In this method, hydrogels containing cells and bioactive components are deposited layer by layer to form constructs that mimic the structural and functional features of native tissues such as cartilage, skin, and vascular networks.[4,5] Hydrogels play an essential role in this process because they provide a hydrated and mechanically supportive microenvironment that enables cell adhesion, proliferation, and differentiation.[6–8] Natural and semi-synthetic polymers, including alginate, gellan gum, hyaluronic acid, collagen, fibrin, and gelatin, have been widely used in this context,[9–12] combined with various cell types ranging from stem cells to patient-specific populations.[13–15]

Despite the increasing sophistication of bioinks and printing strategies, extrusion-based bioprinting continues to face a central limitation. The reproducibility of bioprinted constructs is highly sensitive to the mechanical conditions experienced by the hydrogel during deposition. Parameters such as viscosity, nozzle geometry, temperature, and printing speed influence filament formation, with extrusion pressure playing a particularly critical role. Insufficient pressure generates discontinuous or incomplete deposition, whereas excessive pressure increases shear stress and can compromise cell viability.[16–18] Achieving a balance between structural fidelity and biological performance requires precise control of extrusion pressure together with accurate monitoring of the material's flow behavior.[19–21]

Although these challenges are widely recognized, there are no commercially available tools capable of quantifying extrusion pressure or flow stability in real time during bioprinting.[22,23] As a result, most laboratories still rely on empirical trial-and-error approaches to adjust printing parameters, leading to variability, material waste, and limited comparability between studies.[24] Existing characterization methods, including rheometry, pressure-controlled dispensing systems, or off-line flow tests, do not provide direct information about the pressure thresholds required to initiate extrusion or the pressure range within which continuous and reproducible flow is maintained. This lack of quantitative standards represents a major obstacle for the establishment of reproducible bioprinting workflows and hinders interlaboratory comparability in the field.[25,26]

In addition to laboratory-scale studies, reliable definition and control of extrusion parameters, such as pressure stability and flow consistency, are also relevant when extrusion-based additive manufacturing processes are scaled up. While empirical parameter tuning may be sufficient for small-scale experiments, its effectiveness decreases as workflows become more automated and printing durations increase, leading to higher sensitivity to operator-dependent variability. Recent studies have highlighted the challenges in achieving reproducible bioprinting across different laboratories due to such variability, even under nominally standardized conditions,[27] and have proposed the use of quantitative process parameters, including flow-based metrics, to enhance robustness and comparability.[25] Under these conditions, quantitative approaches that allow the identification of stable operating ranges prior to printing are increasingly important to ensure reproducibility and process consistency in extrusion-based additive manufacturing.[28]

To address this gap, we developed a modular characterization device designed to determine two key parameters under controlled environmental conditions. In addition to extrusion pressure characterization, the proposed platform integrates an environmental control module incorporating temperature, humidity, and carbon dioxide (CO_2) sensing, together with active regulation elements, allowing extrusion parameters to be defined under controlled and reproducible environmental conditions. The first parameter is the minimum extrusion pressure required to initiate hydrogel flow. The second is the stabilization pressure, defined as the pressure range in which the material extrudes continuously and with minimal geometric deviation. The system integrates a pressure sensor, nozzle temperature regulation, and environmental monitoring of temperature, humidity, and CO_2, together with a data acquisition module for real-time recording and analysis. By generating force–displacement curves, the device enables quantitative pre-printing calibration that can be directly applied to commercial bioprinters.

This study validates the platform using 10% gelatin methacryloyl (GelMA), demonstrating that stabilization pressure correlates with improved filament uniformity, grid fidelity, and dimensional accuracy. Furthermore, biological experiments using MCF-7 cells show that operating within the stabilization range reduces shear-induced cell damage. Overall, this work proposes a standardized and sensor-based calibration strategy that enhances process

reproducibility, reduces variability associated with empirical adjustments, and improves the precision and biological performance of extrusion-based bioprinting.

2. Materials and methods

2.1. Materials

Porcine gelatin, methacrylic anhydride, lithium phenyl-2,4,6-trimethylbenzoyl phosphinate, sodium hydroxide, and hydrochloric acid (37%) were obtained from Sigma-Aldrich (US) or Merck (US). Phosphate-buffered saline was purchased from Fisher BioReagents (US). All hydrogels were prepared and loaded using 10 mL sterile polypropylene syringes fitted with 0.22 μm Sterifix® filters (B. Braun, Germany).

For biological validation, human breast adenocarcinoma cell line (MCF-7) were supplied by the Central Research Support Services of the University of Extremadura (Spain). Cells were maintained in high-glucose Dulbecco's Modified Eagle Medium supplemented with 10% fetal bovine serum and 1% penicillin–streptomycin (Gibco, ThermoFisher, US). Cell viability was assessed using the CellTiter 96® AQueous One Solution 3-(4,5-dimethylthiazol-2-yl)-5-(3-carboxymethoxyphenyl)-2-(4-sulfophenyl)-2H-tetrazolium (MTS) kit (Promega, US). Nuclear and viability staining were performed using Hoechst 33342 and propidium iodide (PI) (ThermoFisher, US). All reagents were used as received. Cell-related procedures were performed under sterile conditions in a CO_2-regulated biosafety cabinet.

2.2. Hydrogel preparation

The hydrogel used in this study was based on lyophilized GelMA functionalized at 50%, synthesized from porcine gelatin due to its widespread use in extrusion-based bioprinting, well-documented rheological and biological properties, and its relevance for cell-laden constructs.[29,30] GelMA was obtained through a reaction with methacrylic anhydride, followed by photocrosslinking using lithium phenyl-2,4,6-trimethylbenzoyl phosphinate, a water-soluble photoinitiator commonly employed in bioprinting.[31–33] GelMA's mechanical properties, including swelling, porosity, and modulus, depend on concentration, degree of methacrylation, and ultraviolet (UV) exposure.[33] These parameters influence filament formation and stability during extrusion.

GelMA was synthesized following the protocol reported by Lee *et al.*[34] Briefly, 10% (w/v) type A gelatin was dissolved in phosphate-buffered saline (pH 7.4) at 50°C under continuous stirring. Methacrylic anhydride was added at a 2.2:1 molar ratio relative to primary amines in aliquots of 0.167 mL every 30 min over a period of 3 h. In this established synthesis approach, phosphate-buffered saline acts as a buffering medium, and no active pH adjustment was performed during the methacrylation reaction. The reaction mixture was subsequently dialyzed (12–14 kDa membranes) against deionized water at 40°C for 5 days with twice-daily water changes, and the final product was lyophilized.

For bioprinting experiments, GelMA was reconstituted at 10% (w/v), a concentration widely reported for extrusion-based bioprinting that provides a balance between viscosity and post-crosslinking mechanical stability.[32,35,36] Solutions were sterilized by filtration (0.22 μm) and heated at 50°C for 60 min under agitation to ensure complete dissolution and homogeneity. Prior to bioprinting, the pH of the reconstituted GelMA solution was adjusted to physiological values (pH 7.0–7.4) using sterile sodium hydroxide or hydrochloric acid to ensure material stability and cell compatibility. Cells were encapsulated in the GelMA hydrogel at a density of 1×10^6 cells/mL for all bioprinting experiments.

2.3. *In vitro* validation

2.3.1. Cell culture

MCF-7 cells (ATCC® HTB-22™) were cultured in high-glucose Dulbecco's Modified Eagle Medium with GlutaMAX supplemented with 10% fetal bovine serum and 1% penicillin–streptomycin, and maintained at 37°C in a humidified atmosphere with 5% CO_2. Subconfluent monolayers were passaged using trypsin-ethylenediaminetetraacetic acid and expanded in 75 cm^2 culture flasks.

For cytotoxicity and cell validation assays, cells were seeded in multiwell plates at a density of 10,000 cells per well and allowed to adhere under standard culture conditions prior to experimental exposure. Cell density was controlled by using a fixed seeding density and standardized incubation times.

2.3.2. MTS assay

Cytotoxicity of GelMA prior to extrusion was evaluated using the CellTiter 96® AQueous MTS assay. Cells were seeded in 96-well plates, exposed to GelMA for 24 or 48 h, and incubated with 20 μL of the reagent in 100 μL medium for 4 h. Absorbance at 490 nm was recorded to quantify metabolic activity.

2.3.3. Confocal microscopy

Cells were seeded in 8-well chamber slides either without hydrogel (controls) or embedded in GelMA for extrusion at experimental pressures. After 24 h of incubation, cells were stained with Hoechst 33342 (0.0005%) and PI (10 μg/mL) for 30 min. Imaging was performed using an Olympus (Japan) Fluoview FV1000 confocal microscope with a 10× objective.

2.4. Development of a device for parameter optimization and control in extrusion-based three-dimensional bioprinting

Extrusion bioprinting accuracy depends on extrusion pressure, plunger velocity, hydrogel temperature, and environmental conditions (temperature, humidity, and CO_2). A modular device was developed to quantify these variables in real time and determine the minimum extrusion pressure and stabilization pressure for controlled hydrogel flow.

The system described in this section was conceived as an independent and modular characterization device that integrates mechanical actuation, pressure sensing, temperature regulation, and environmental monitoring into a single platform aimed at quantitatively characterizing extrusion behavior prior to bioprinting. By decoupling material characterization from the printing process, the device enables systematic identification of minimum extrusion and stabilization pressure ranges, which can be directly transferred to different extrusion-based bioprinting systems. This modular architecture allows device-independent calibration, improves reproducibility, and facilitates adaptation to different hydrogel formulations and extrusion configurations.

2.4.1. Design principles

The system comprises three coordinated modules:

i Extrusion module: Integrates stepper motors, force/pressure sensors, and a nozzle-temperature probe to quantify extrusion dynamics and regulate hydrogel temperature.

ii Environmental control module: Maintains stable printing conditions via temperature, humidity, and CO_2 sensors, supplemented with actuators such as a heating unit, humidifier, and UV-C disinfection system.

iii Processing and control module: Collects real-time data from all sensors through a microcontroller and provides visualization, parameter adjustment, and optional high-resolution imaging for monitoring flow behavior and gelation.

The design prioritizes reproducibility, quantification, and adaptability to commercial bioprinting workflows.

2.4.2. Parameters calculated by the device

The characterization platform enables the determination of a set of quantitative parameters that describe the extrusion behavior of hydrogels under controlled thermal and environmental conditions. The device directly measures the axial force applied to the syringe plunger and records plunger displacement as a function of time, from which relevant extrusion parameters are derived.

First, the system determines the minimum extrusion pressure (P_min), defined as the lowest pressure at which sustained and continuous material flow is first detected at the nozzle outlet. The extrusion pressure (P) is calculated from the axial force (F) applied to the syringe plunger and the effective cross-sectional area of the syringe (A), as shown in **Equation (1)**:

$$P = \frac{F}{A} \tag{1}$$

The minimum extrusion pressure marks the transition from a static (no-flow) regime to a dynamic flow regime, but does not necessarily ensure stable or reproducible filament deposition.

Second, the device identifies the stabilization pressure (P_stab), defined as the pressure range in which the extrusion force remains stable over time and filament deposition becomes continuous, homogeneous, and reproducible. This stabilization window is identified experimentally from the force–displacement curves as the region in which the force signal reaches a steady plateau, characterized by an approximately constant slope and low-amplitude oscillations within predefined tolerances, indicating steady-state extrusion. The stabilization force is determined for each extrusion velocity, enabling comparison across different printing conditions.

Third, the device records plunger displacement as a function of time, from which the extrusion displacement rate is obtained. The corresponding volumetric flow rate (Q) is estimated from the plunger displacement velocity (v) and the syringe cross-sectional area (A) using **Equation (2)**:

$$Q = v \times A \tag{2}$$

Finally, the system records nozzle temperature and environmental variables (temperature, humidity, and CO_2) in real time. These parameters are monitored to ensure that extrusion behavior is evaluated under stable and reproducible conditions and to detect thermal or environmental drifts that could influence hydrogel viscosity and flow behavior.

Taken together, these measurements provide a rigorous and quantitative framework for defining the mechanical conditions required to initiate hydrogel flow, identify stabilization pressure as a function of extrusion velocity,

maintain stable extrusion, and achieve reproducible filament deposition.

2.4.3. System architecture

The device architecture (Table 1) includes: (i) an extrusion unit with stepper-controlled plunger movement, temperature regulation (±0.5°C), and a pressure sensor (±2% accuracy); (ii) a sealed environmental chamber fabricated from polylactic acid supports and methacrylate panels, ensuring stable temperature, humidity, and CO_2 levels; (iii) UV-C disinfection prior to loading; and (iv) a microcontroller enabling synchronization of sensor readings, storage of extrusion data, and photographic documentation for traceability.

The CO_2 sensor functions solely as a monitoring tool, verifying that environmental conditions remain within physiologically relevant ranges, without integrated gas injection. The system operates independently from commercial bioprinters, serving as a pre-printing characterization platform that defines optimal parameters transferable to extrusion-based devices.

2.4.4. Device operation

The device operates from an initial extrusion pressure set according to the type of bioink/hydrogel. The pressure sensor monitors pressure changes in real time, and the thermal sensor maintains the optimal temperature of the bioink/hydrogel to prevent premature solidification or cell damage. Before bioprinting begins, UV-C disinfection is activated, and the chamber is preheated to the optimal temperature. During printing, the humidity and CO_2 sensors adjust to replicate physiological conditions.

Table 1. Representation of the modular device for extrusion-based bioprinting

Module	Components
Extrusion module	Force sensor (0–196.1 kPa)
	Thermal thermistor (−50 to 150°C)
	Polyimide film heater (Up to 180°C)
	Stepper motors
	Displacement meter (0–155 mm)
Environmental control module	Ultraviolet sterilization
	Temperature control
	Humidity control
	Carbon dioxide control
Processing and control module	NodeMCU V3
	Web

Note: The system consists of three functional units: (i) an extrusion module equipped with stepper motors, a pressure sensor, and a nozzle temperature probe; (ii) an environmental control module containing sensors for temperature, humidity, and CO_2, together with actuators such as a heating unit, humidifier, and UV-C disinfection system; and (iii) a data acquisiti on and control module that integrates all sensors into a microcontroller for real-time monitoring and parameter adjustment. In the diagram, measurement components (sensors) are distinguished from control units (motors, heating elements, and actuators) to clarify their respective roles in process monitoring and regulation.

The above process is shown schematically in Figure 1, and begins with disinfection using the UV light module (Figure 1C-i). Subsequently, the bio-ink/hydrogel loaded in a syringe is introduced into the base designed for this purpose (Figure 1C-ii), and a series of load cell movement speeds are pre-set in the equipment (Figure 1C-iii). Finally, the load cell begins its descent at the pre-set speed and will maintain this speed throughout the test (Figure 1C-iv). The load cell will record the force required for the material to start to come out, as well as the temperature of the hydrogel and the temperature of the chamber.

The proposed device allows the measurement of extrusion pressure and printing speed according to the displacement of the syringe plunger, as well as the control of temperature, humidity, and CO_2 concentration. To do this, the new equipment developed integrates high-precision sensors and control systems to monitor and adjust the bioprinting parameters in real time. All these features enable data recording and storage, full traceability of printing conditions, real-time parameter adjustment and visualization, and compatibility with commercial bioprinters through a modular design adaptable to different systems.

2.4.5. Device calibration and validation

The device was calibrated and validated under experimental conditions. For the calibration of the force sensor, a universal testing machine equipped with a certified load cell (±0.5% accuracy; Instron, US) was used; the temperature sensor was calibrated against a certified thermocouple in different temperature ranges. Finally, the CO_2 sensor was validated using certified standard mixtures. The following experimental methodology was proposed to validate the device:

i Measurement accuracy: Extrusion tests were analyzed by comparing measured force-derived pressures with values estimated by numerical image-based analysis (AutoCAD, 2025). Structural fidelity of printed constructs was assessed using the structural similarity index (SSIM) after grayscale conversion, Gaussian filtering, Canny edge detection, and contour comparison.

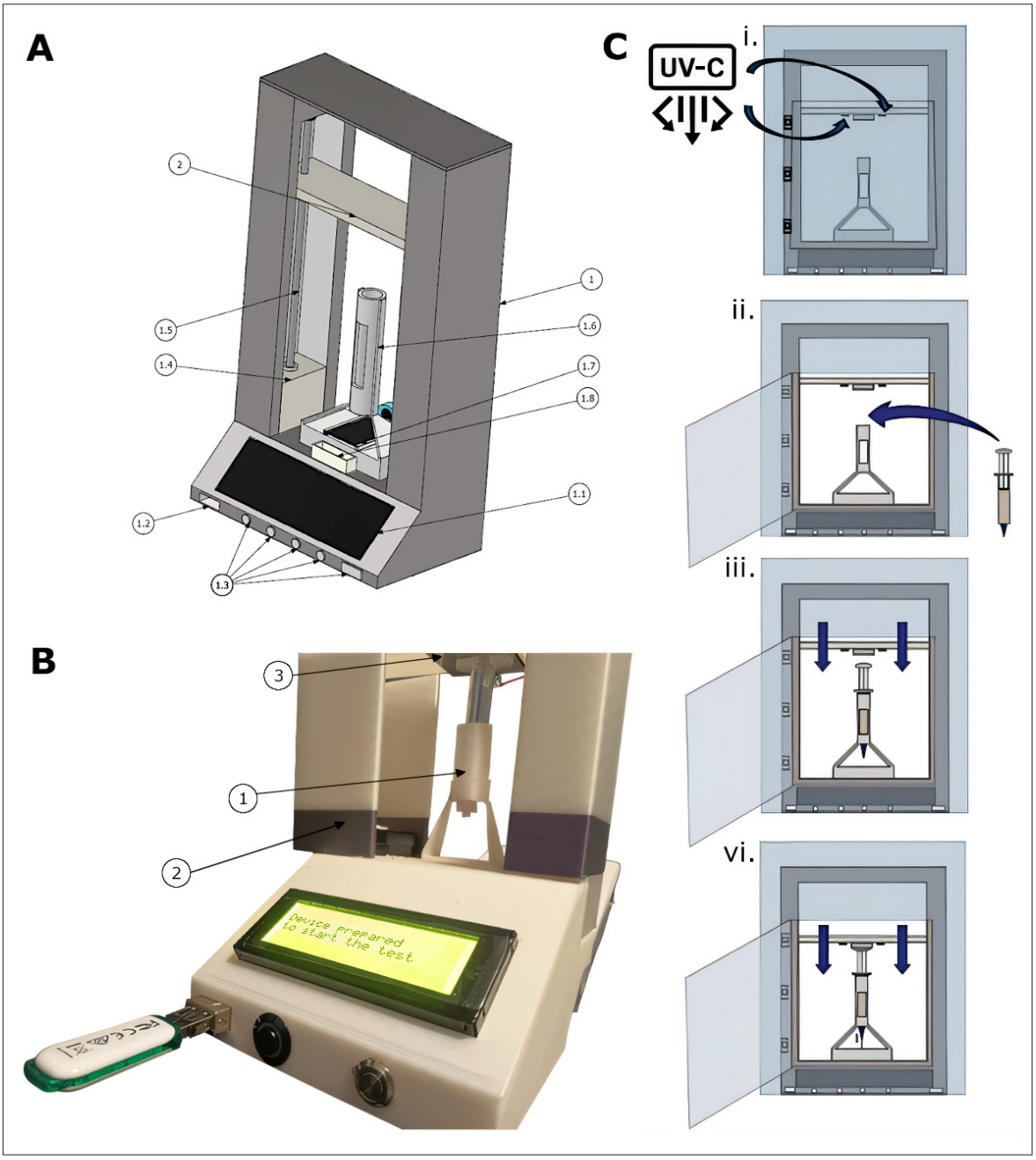

Figure 1. Overview of the modular characterization platform and its operation. (A) Schematic representation of the device showing the main components: (1) main structural frame of the device; (1.1) control display; (1.2) USB input/output ports; (1.3) control button panel; (1.4) motor; (1.5) lead screws; (1.6) heated support; (1.7) conveyor belt; (1.8) removable drawer; and (2) mobile platform. (B) Photograph of the physical prototype of the characterization device integrating the main sensing and control elements: (1) polyimide (PI, 12 V) film electric heater embedded in the nozzle holder for temperature regulation, combined with an exposed-tip 10 kΩ negative temperature coefficient thermistor for local temperature sensing; (2) linear displacement measurement system based on a capacitive encoder located next to the stepper motor for real-time tracking of plunger position; and (3) a force sensitive resistor (FSR) for estimating the load during extrusion. (C) Schematic workflow of device operation: (i) chamber disinfection using an ultraviolet (UV)-C lamp (280 nm, 5 V) before loading; (ii) insertion of gelatin methacryloyl hydrogel into the syringe; (iii) pre-setting of plunger displacement speed; and (iv) extrusion test showing hydrogel flow while simultaneously recording pressure and temperature. All experiments were conducted under closed-chamber conditions to ensure environmental stability and reproducibility.

ii Environmental stability: Chamber stability was evaluated during a 6-h continuous operation, confirming temperature (37°C ± 0.5°C), humidity (80% ± 5%), and CO_2 levels (5% ± 0.2%).

iii Impact on cell viability: GelMA constructs were extruded under two conditions: over-extrusion pressure and stabilization pressure (optimal).

Cells embedded in each construct were stained and quantified to assess viability after extrusion. All experiments included sensor verification, hydrogel loading, initial pressure adjustment, extrusion monitoring, and post-printing viability analysis.

2.5. Statistical analysis

All quantitative data are reported as mean ± standard deviation. Filament deflection measurements were obtained from three independent printing replicates for each extrusion pressure condition (n = 3). Grid fidelity was evaluated through quantitative image-based analysis by comparing theoretical and experimentally printed void areas.

Cell viability assays were performed using duplicate plates with triplicate wells per condition (n = 6), and results are presented as relative viability values with associated standard deviation. No inferential statistical tests were applied, as the analysis focused on descriptive comparison of extrusion pressure conditions and quantitative assessment of geometric and biological trends.

Image-based measurements, including filament deflection, void area analysis, and SSIM, were performed using Fiji (version 2.9.0)/ImageJ (version 1.54p).

3. Results and discussion

3.1. Device validation during extrusion-based bioprinting

The device was calibrated according to the procedures described in **Section 2.4.5** and validated through a series of controlled extrusion experiments to assess its ability to monitor pressure dynamics and identify stable operating conditions for hydrogel bioprinting. Continuous force and pressure readouts allowed real-time detection of deviations from the expected stabilization profile, revealing events such as viscosity fluctuations, entrapped air, or the onset of nozzle obstruction. Nozzle temperature remained within ±0.5°C of the setpoint, ensuring consistent rheological behavior of GelMA and preventing premature gelation. Environmental parameters (temperature, humidity, and CO_2) were also maintained within narrow tolerances, reducing external variability that is known to influence hydrogel viscosity and cell viability.

Extrusion tests with 10% GelMA at 37°C using a 22G nozzle and plunger speeds of 1, 5, 10, and 20 mm/min produced characteristic force–displacement curves (Figure 2), which consistently exhibited three distinct regions: (i) an initial compaction phase, (ii) a transient relaxation phase associated with flow initiation, and (iii) a steady-state plateau corresponding to continuous extrusion. Maximum and stabilization forces extracted from these curves are summarized in Table 2. This behavior reflects the viscoelastic and shear-thinning nature of GelMA, where a yield stress must be exceeded before stable flow is established.

During the initial compaction phase, force increases without measurable plunger displacement, indicating compression of the hydrogel and system compliance prior to material release. The onset of extrusion is identified at the point where the force increase is accompanied by displacement (Figure 2), marking the minimum extrusion forcepreceding the stabilization regime.

In this context, stable flow is experimentally demonstrated by the presence of a well-defined steady-state plateau in the force–displacement curves (Figure 2), together with the reproducible stabilization pressure identified across different plunger speeds (Figure 3). These features indicate continuous and homogeneous extrusion under constant mechanical conditions and provide a quantitative reference for stable material flow.

A clear positive correlation was observed between the speed and both maximum and stabilization forces, reflecting the increased energy required to sustain higher volumetric flow rates. Among these parameters, stabilization force emerged as the most informative, as it defined the onset of continuous, homogeneous extrusion and correlated directly with filament uniformity and print quality observed in subsequent printing tests. Conversion of force values into extrusion pressures (Figure 3) enabled the identification of a reproducible stabilization zone, consistent with the shear-thinning behavior of GelMA hydrogels. Operating within this pressure range minimized both under-extrusion (insufficient pressure to overcome yield stress) and over-extrusion (filament swelling and geometric deviation), thereby improving reproducibility across printing conditions and providing a quantitative basis for extrusion parameter selection rather than relying on empirical adjustments.

Environmental stability tests confirmed that the chamber maintained 37°C ± 0.5°C, 80% ± 5% humidity, and 5% ± 0.2% CO_2 throughout the experiments. This control is relevant because small deviations in temperature or humidity can alter hydrogel viscosity, crosslinking kinetics, and cell survival during bioprinting.[37,38] By

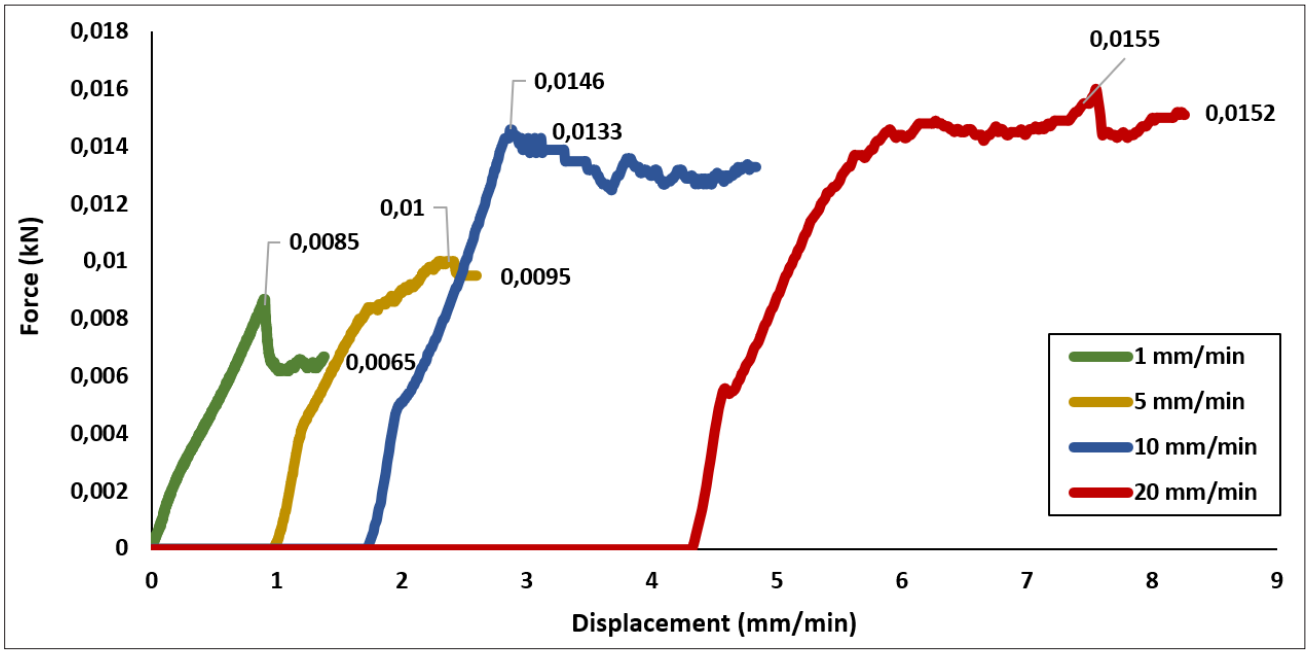

Figure 2. Force–displacement curves obtained during extrusion tests with 10% gelatin methacryloyl hydrogel at 37°C using a 22G nozzle and plunger speeds of 1, 5, 10, and 20 mm/min. Each curve shows the maximum force required to initiate extrusion and the stabilization force corresponding to continuous filament flow. The three characteristic phases of the process (initiation, transient, and stabilization) are indicated. These data were used to calculate stabilization pressures for subsequent experiments.

Table 2. Force values based on Figure 2

Applied speed (mm/min)	Peak force (kN)	Stabilization force (kN)
1	0.0085	0.0065
5	0.01	0.0095
10	0.0146	0.0133
20	0.0155	0.0152

ensuring that extrusion behaviour is measured under stable conditions, the device enables reproducible determination of pressure thresholds across different hydrogel batches and formulations.

It is important to note that the main challenge in extrusion-based bioprinting is not solely to measure pressure, but to achieve stable and reproducible flow. Instabilities may arise from plunger dynamics, flow inertia, or microstructural heterogeneities within the hydrogel. Although the device does not mechanically eliminate these sources of variability, its real-time pressure–displacement monitoring enables early detection of irregularities and facilitates the identification of the stabilization pressure. This quantitative reference mitigates inconsistencies in filament deposition and supports reproducible printing across a range of materials and operating conditions.

3.2. Device validation by printing of test structures

Once the optimal extrusion pressure was identified from the force–displacement and pressure–speed analyses (Figure 3), its effectiveness was validated experimentally by printing 10% GelMA hydrogels under controlled conditions. For the printing speed selected for subsequent experiments (10 mm/min), the device identified a stabilization pressure of 165 kPa. The stabilization pressure was defined as the pressure reported by the device at which a continuous and steady filament was obtained. Under- and over-extrusion conditions were experimentally validated by selecting pressures below (155 kPa) and above (185 kPa) this value and confirming their effects through filament morphology and dimensional deviation.

3.2.1. Printing of single filaments

To evaluate the effect of extrusion pressure on filament morphology, linear test structures were printed at a constant speed of 10 mm/min under three pressure conditions: (i) under-extrusion: pressure below the optimal range (155 kPa), (ii) over-extrusion: pressure above the optimal range (185 kPa), and (iii) optimal extrusion: stabilization pressure determined by the device (165 kPa).

Representative filaments are shown in Figure 4. Under-extrusion generated discontinuous and low-profile strands (1.46–1.95 mm), reflecting insufficient

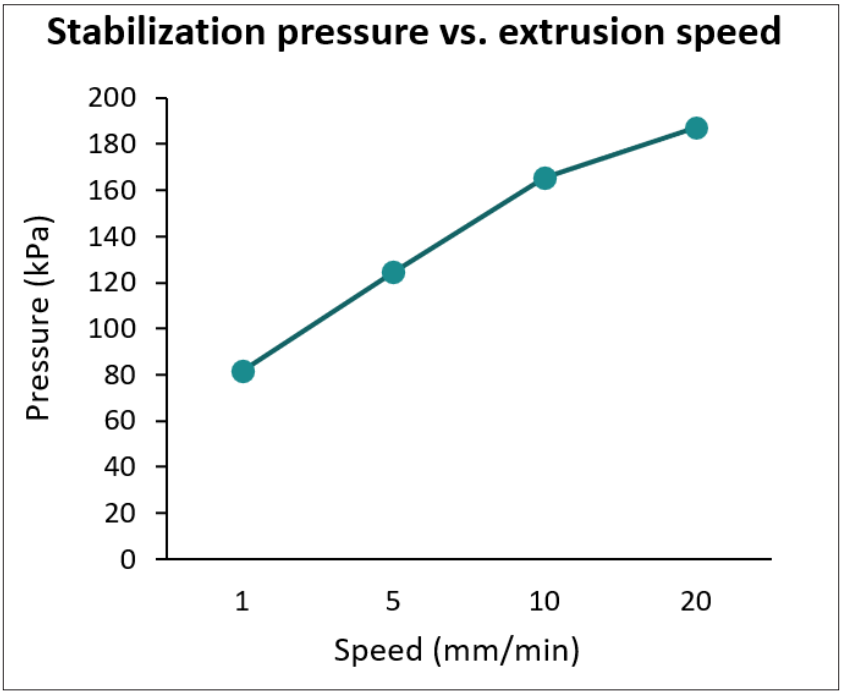

Figure 3. Stabilization pressure as a function of plunger speed for 10% gelatin methacryloyl hydrogel at 37°C with a 22G nozzle. Results show the shear-thinning behavior of the material, with continuous and stable flow achieved within the stabilization zone (highlighted region). Operating in this range minimizes under- and over-extrusion defects.

force to sustain continuous hydrogel flow. Over-extrusion produced swollen, irregular filaments (2.34–2.84 mm) due to excessive discharge and loss of geometric control. In contrast, extrusion at 165 kPa yielded continuous, homogeneous filaments with well-defined geometry (1.99–2.45 mm), demonstrating the stability of flow within the determined pressure window.

To quantify filament uniformity, deflection measurements were obtained for each condition (Table 3). Under-extrusion exhibited the lowest average deflection (1.58 mm), consistent with reduced material deposition, whereas over-extrusion showed the highest values (2.78 mm), corresponding to excessive thickness and poorer structural stability. Extrusion at the stabilization pressure resulted in intermediate but significantly more uniform deflection (2.22 mm; coefficient of variation < 10%), confirming a more consistent and controlled deposition profile.

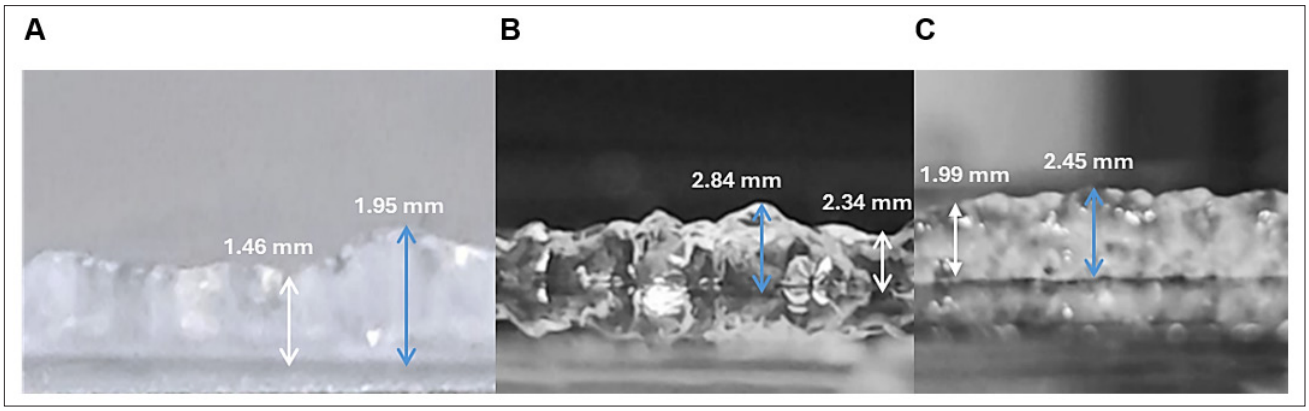

Figure 4. Bioprinted filaments obtained with 10% gelatin methacryloyl hydrogel at 37°C and 10 mm/min extrusion speed using a 22G nozzle. (A) Under-extrusion at 155 kPa resulted in discontinuous and low-profile filaments (1.46–1.95 mm height). (B) Over-extrusion at 185 kPa produced irregular, swollen filaments (2.34–2.84 mm height). (C) Extrusion at stabilization pressure (165 kPa) yielded continuous and homogeneous filaments (1.99–2.45 mm height). These results confirm the relevance of operating within the stabilization range for uniform hydrogel deposition.

Table 3. Deflection measurements of GelMA filaments printed at different pressures

Pressure condition	Pressure (kPa)	Speed (mm/min)	Maximum deflection (mm)	Minimum deflection (mm)	Average deflection (mm)	Standard deviation (mm)	% coefficient of variation
Low pressure	155	10	1.95	1.46	1.58	0.14	8.9
High pressure	185	10	2.84	2.34	2.78	0.06	2.2
Optimum pressure	165	10	2.45	1.99	2.22	0.21	9.5

Note: Values represent the mean ± standard deviation of three independent replicates (n = 3). The coefficient of variation was below 10% in all cases, confirming the repeatability of the measurements.

These results demonstrate that extrusion pressure is a key determinant of filament morphology and print quality. Operating within the stabilization range maximises filament uniformity, minimises dimensional deviation, and provides reproducible output across replicates. This behavior is consistent with previous reports that describe the strong dependence of filament geometry on extrusion pressure in shear-thinning hydrogels.[39] The observed improvements in filament consistency validate the device's ability to identify pressure conditions that ensure stable gel flow and reliable deposition during extrusion-based bioprinting.

3.2.2. Printing of grid structures using 10% gelatin methacryloyl hydrogel

3.2.2.1. Qualitative evaluation

A grid structure was designed in Inventor (Autodesk Inventor 2025) (Figure 5) to evaluate the effect of extrusion pressure on printability and reproducibility. Printing was carried out under three pressure conditions: 145 kPa (under-extrusion), 185 kPa (over-extrusion), and 165 kPa (stabilization pressure identified by the device). Grid-based printing tests are widely used to evaluate hydrogel printability, as they highlight filament continuity, line width uniformity, and the ability to reproduce the intended geometry.[40,41]

Based on qualitative visual assessment (Figure 5), print fidelity was considered highest at 165 kPa. At this pressure, filaments appeared continuous and homogeneous, with a more uniform line width and improved preservation of the designed grid geometry. In particular, compared with other pressure conditions, the structure printed at 165 kPa exhibited better-defined filaments relative to the nozzle gauge used, resulting in clearer separation between adjacent lines and more regular square features.

At 145 kPa, the applied pressure was insufficient to maintain continuous extrusion. Filaments appeared discontinuous, fragmented, and irregular, compromising structural reproducibility. At 185 kPa, excessive pressure led to over-extrusion, resulting in swollen filaments, partial occlusion of narrow voids, and loss of geometric precision due to uncontrolled material accumulation.

These observations demonstrate that printing within the stabilization pressure range ensures sufficient force to overcome the material yield stress while preventing excessive discharge. The results reinforce the role of stabilization pressure as a critical parameter for achieving reproducible and high-quality bioprints, in agreement with previous studies reporting pressure-dependent variations in filament morphology.[42,43]

3.2.2.2. Quantitative evaluation

This section provides a quantitative assessment of the printing fidelity of the hydrogel by comparing the theoretical and actual void areas of the printed grids obtained at two different pressures (165 kPa and 185 kPa). This analysis represents the first quantitative benchmark of printing accuracy using a simple test geometry, prior to evaluating pressure effects on more complex 3D structures in the following section.

To quantitatively assess grid fidelity, theoretical areas were compared with the corresponding experimentally measured areas at two pressure conditions: 165 kPa (stabilization) and 185 kPa (over-extrusion). Detailed values are shown in Tables 4 and 5, and a summary is provided in Table 6.

Similarity values were calculated as the ratio between the theoretical area (A_t) and the experimentally measured area (A_r), expressed as a percentage, according to **Equation (3)**:

$$Similarity\ (\%) = \left(\frac{Ar}{At}\right) \times 100 \quad (3)$$

Values closer to 100% indicate a higher agreement between the designed and printed structures. At 165 kPa, similarity values ranged from ≈38.46% to ≈89.74%, with

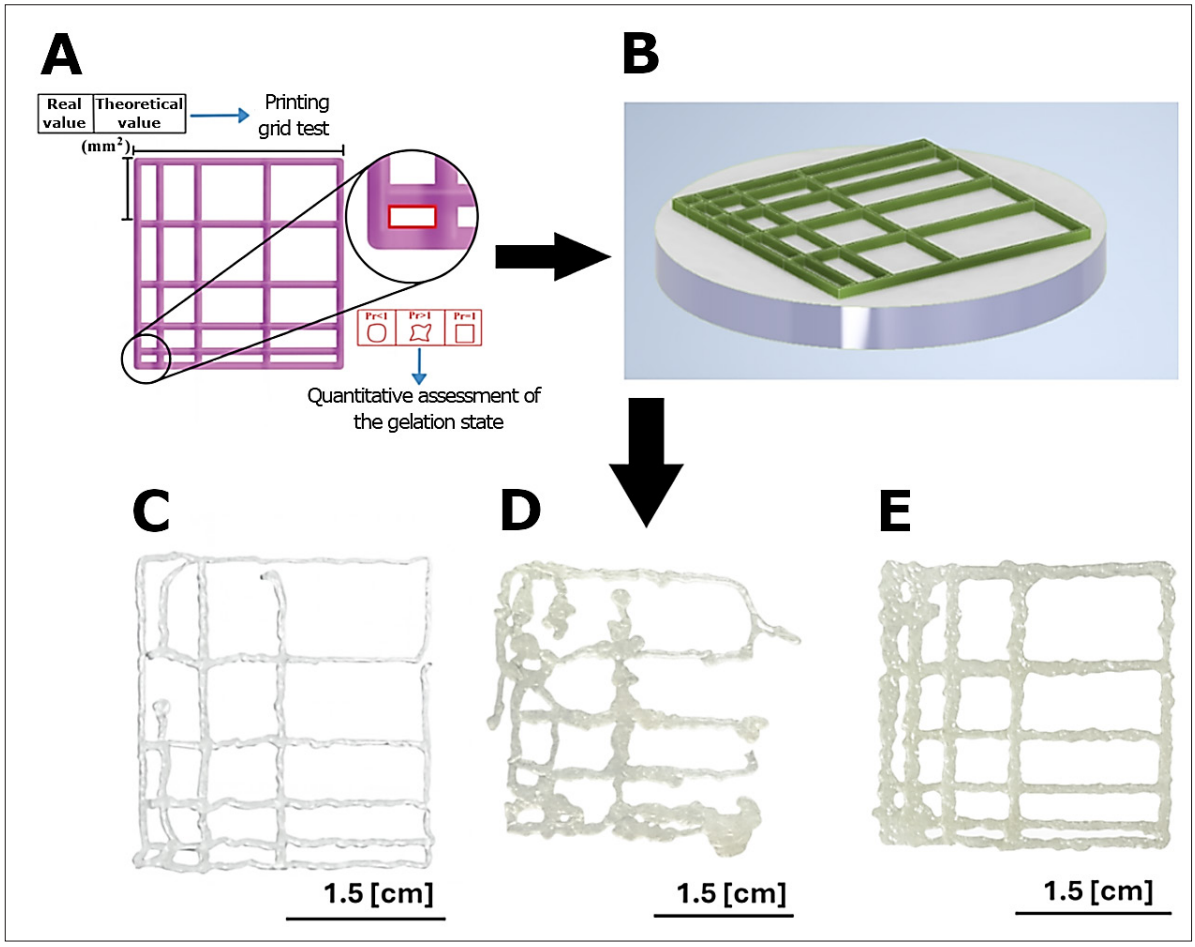

Figure 5. Determination of the degree of printability of a hydrogel using a bioprinted grid [40]. (A) The grid was designed using the Inventor software and subsequently saved as an .stl file, ensuring compatibility with the three-dimensional bioprinter for seamless printing. (B) Grid structures were printed with 10% GelMA hydrogel at 37°C and 10 mm/min using a 22G nozzle. (C) Under-extrusion at 145 kPa produced incomplete and discontinuous filaments. (D) Over-extrusion at 185 kPa caused swelling and loss of geometric fidelity. (E) Stabilization pressure (165 kPa) yielded homogeneous filaments and well-defined grid geometry. Scale bar: 1.5 cm. These results highlight the impact of extrusion pressure on print fidelity.

an overall similarity of ≈63.15%. Larger voids exhibited the highest similarity, consistent with the lower sensitivity of large features to small filament deviations.

At 185 kPa, similarity values ranged from 0% to ≈80.10%, with an overall similarity of ≈51.25%. The lower similarity was largely due to material accumulation and filament swelling, which led to partial occlusion of smaller voids and increased deviation in larger ones.

Overall, printing at the stabilization pressure reduced global area deviation (1.51 cm^2 vs. 1.99 cm^2) and improved geometric accuracy, reflected in a closer agreement between theoretical and experimentally measured void areas, reduced variability among voids within the same structure, and minimized geometric distortion associated with filament swelling or partial void occlusion. These results confirm that the stabilization pressure determined by the device constitutes a quantitative threshold that enhances the reproducibility and geometric fidelity of printed grid structures.

To explore the relevance of stabilization pressure in more demanding geometries, a biomimetic 3D heart model (Figure 6A) was printed at 165 kPa (stabilization pressure) and 185 kPa (over-extrusion). This model was selected due to its fine features, curved surfaces, and nonuniform thickness, which make it particularly sensitive to deviations in flow rate and layer stacking.

Printing at 185 kPa led to structural failure (Figure 6B). Excessive extrusion produced filament swelling and accumulation between layers, causing nozzle entrapment and collapse of the construct. This failure mode indicates

Table 4. Theoretical and actual area values corresponding to the designed and printed grids, respectively, at the stabilization pressure of 165 kPa

Number	Theoretical area (cm^2)	Real area (cm^2)	Difference	% Similarity[a]
1	1.040	0.900	0.140	86.538
2	0.832	0.650	0.182	78.134
3	0.624	0.510	0.114	81.731
4	0.416	0.320	0.096	76.979
5	0.208	0.100	0.108	48.077
6	0.520	0.430	0.090	82.676
7	0.416	0.300	0.116	72.115
8	0.312	0.220	0.092	70.490
9	0.208	0.150	0.058	72.150
10	0.104	0.050	0.054	48.077
11	0.260	0.120	0.140	46.154
12	0.208	0.180	0.028	86.538
13	0.156	0.140	0.016	89.744
14	0.104	0.090	0.014	86.622
15	0.052	0.020	0.032	38.462
16	0.130	0.060	0.070	46.118
17	0.104	0.035	0.069	33.816
18	0.078	0.025	0.053	32.051
19	0.052	0.025	0.027	48.077
20	0.026	0.010	0.016	38.462

Note: [a]Minor discrepancies in the calculated similarity values are due to rounding of the reported area measurements.

Table 5. Theoretical and actual area values corresponding to the designed and printed grids, respectively, at the over-extrusion pressure of 185 kPa

Number	Theoretical area (cm^2)	Real area (cm^2)	Difference	% Similarity[a]
1	1.040	0.810	0.230	77.885
2	0.832	0.600	0.232	72.124
3	0.624	0.490	0.134	78.526
4	0.416	0.220	0.196	52.923
5	0.208	0.110	0.098	52.885
6	0.520	0.390	0.130	74.986
7	0.416	0.290	0.126	69.712
8	0.312	0.250	0.062	80.103
9	0.208	0.120	0.088	57.720
10	0.104	0.040	0.062	38.462
11	0.260	0.190	0.070	73.077
12	0.208	0.110	0.098	52.885
13	0.156	0.050	0.106	32.051
14	0.104	0.040	0.064	38.499
15	0.052	0.020	0.032	38.462
16	0.130	0.050	0.080	38.432
17	0.104	0.040	0.064	38.647
18	0.078	0.030	0.048	38.462
19	0.052	0.010	0.042	19.231
20	0.026	0.000	0.026	0.000

Note: [a]Minor discrepancies in the calculated similarity values are due to rounding of the reported area measurements.

Table 6. Comparative analysis of the results corresponding to the grating areas at two different pressures

Pressure	Measurements	Values
165 kPa	% Similarity	63.151
	Theoretical area (cm^2)	5.849
	Printed area (cm^2)	4.335
	Area difference (cm^2)	1.514
185 kPa	% Similarity	51.253
	Theoretical area (cm^2)	5.849
	Printed area (cm^2)	3.860
	Area difference (cm^2)	1.989

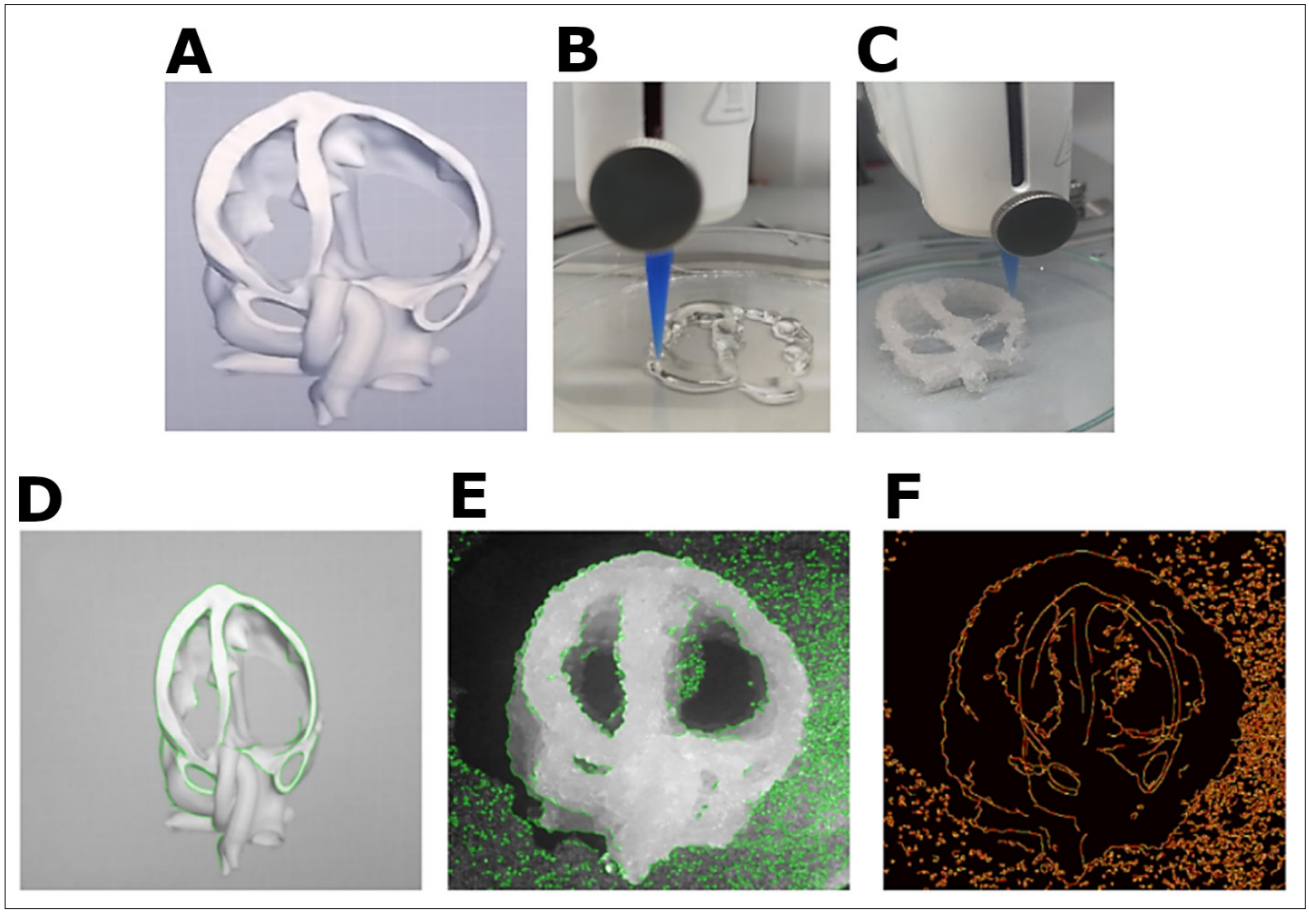

Figure 6. Bioprinting process and evaluation of pressure optimization. (A) Reference three-dimensional (3D) model used for bioprinting. (B) Attempted bioprinting at 185 kPa, where excessive material extrusion caused structural collapse. (C) Bioprinting was performed using the optimized extrusion pressure, enabling the complete reproduction of the model without significant structural defects. The process was carried out using a BIO X bioprinter (CELLINK), with extrusion pressure parameters defined on the basis of calibration results obtained using the custom-developed characterization device, followed by a final ultraviolet-mediated crosslinking step. Next, a comparison was made between the digital reference model and the pressure-stabilized printed structure (165 kPa). (D) Digital reference heart model. (E) Bioprinted construct. (F) Computational overlay showing contour alignment and deviations used to calculate the structural similarity index (0.63). This analysis demonstrates that optimized extrusion conditions enhance the fidelity of complex 3D structures.

a mismatch between extrusion flow rate, layer height, and material consolidation, typical of over-extrusion conditions.

In contrast, printing at 165 kPa (Figure 6C) produced a complete and structurally coherent construct that preserved global contours and major anatomical features of the reference model. Although some local irregularities remained in thin or unsupported regions, the overall morphological fidelity was significantly higher at the optimal pressure.

A contour-based comparison (Figure 6D–F) was performed by overlaying the digital model and the printed construct, enabling calculation of the SSIM (0.63). This value is consistent with the fidelity trends observed in the grid structures and confirms that optimized pressure enhances dimensional accuracy and global correspondence in complex 3D geometries.

Together, these results demonstrate that the stabilization pressure identified by the device is essential not only for simple planar patterns but also for complex architectures. By minimizing filament swelling, regulating material output, and improving layer alignment, optimal extrusion pressure ensures greater geometric fidelity, enhances construct completeness, and reduces printing defects across multiple levels of structural complexity.

3.3. *In vitro* validation

In vitro validation was performed to assess both the intrinsic biocompatibility of the hydrogel and the effect of extrusion pressure on cell viability. Two complementary approaches were used: an MTS assay to evaluate baseline cytocompatibility of the material and confocal live/dead imaging to assess post-printing viability under different pressure conditions.

3.3.1. MTS assay

Extrusion-based bioprinting exposes cells to mechanical stress generated by pressure-driven flow and by the rheological properties of the hydrogel. Before analysing the effect of the extrusion process itself, it is essential to confirm that the hydrogel used as a bioink does not introduce cytotoxic effects that could confound subsequent viability analyses.

To evaluate baseline biocompatibility, an MTS assay was performed using 10% GelMA without extrusion. Cells were cultured on the hydrogel for 24 and 48 h, and metabolic activity was quantified by absorbance at 490 nm (Figure 7).

The results showed viability values of 113% at 24 h and 116% at 48 h relative to the control, indicating that GelMA did not exert cytotoxic effects under the tested conditions. These findings confirm that the material is suitable for subsequent extrusion studies, ensuring that observed viability changes can be attributed to bioprinting conditions rather than to intrinsic hydrogel toxicity.

3.3.2. Confocal microscopy

During extrusion, cells are exposed to shear forces that may compromise viability, particularly when printing at high pressures or with viscous hydrogels. Previous studies have identified shear stress within the nozzle as one of the main contributors to cell damage during extrusion.[44]

To assess the impact of extrusion pressure, GelMA constructs containing cells were printed at 165 kPa (stabilization pressure) and 185 kPa (over-extrusion). Immediately after printing, samples were stained with Hoechst 33342 (nuclei) and PI (non-viable cells) and imaged using confocal microscopy (Figure 8). Cells treated with 10 mM hydrogen peroxide were included as a positive control to confirm PI staining of non-viable cells. Cell viability was quantified using Fiji/ImageJ according to **Equation (4)**:

$$Cell\ viability\ (\%) = \frac{Live\ cells}{Live\ cells + Dead\ cells} \cdot 100\% \qquad (4)$$

At 165 kPa, viability reached 97.98%, whereas at 185 kPa, it decreased to 88.57%. Both values fall within ranges considered acceptable for extrusion bioprinting, although the reduction observed at 185 kPa suggests that pressures above the stabilization zone begin to impose measurable mechanical stress on cells.

These results are consistent with previous reports. Ning *et al.*[45] showed that cell viability generally remains high when printing below 200 kPa, with less than 20% cell death even at pressures approaching 400 kPa when using alginate bioinks. In the present study, both extrusion pressures fall within this safe range, and the viability values obtained corroborate the suitability of the printing conditions.

Overall, the data confirm that extrusion at the stabilization pressure (165 kPa) maximizes cell survival, while operation at 185 kPa introduces additional mechanical stress but still supports high viability. These findings validate the extrusion parameters identified by the device and reinforce the importance of operating within the stabilization zone to minimize cell damage.

Long-term cell survival in GelMA-based scaffolds has been widely reported in the literature under appropriate culture conditions. Previous studies using extrusion-based bioprinting have shown that when extrusion parameters are maintained within suitable ranges, high cell viability can be sustained over several days of culture, indicating

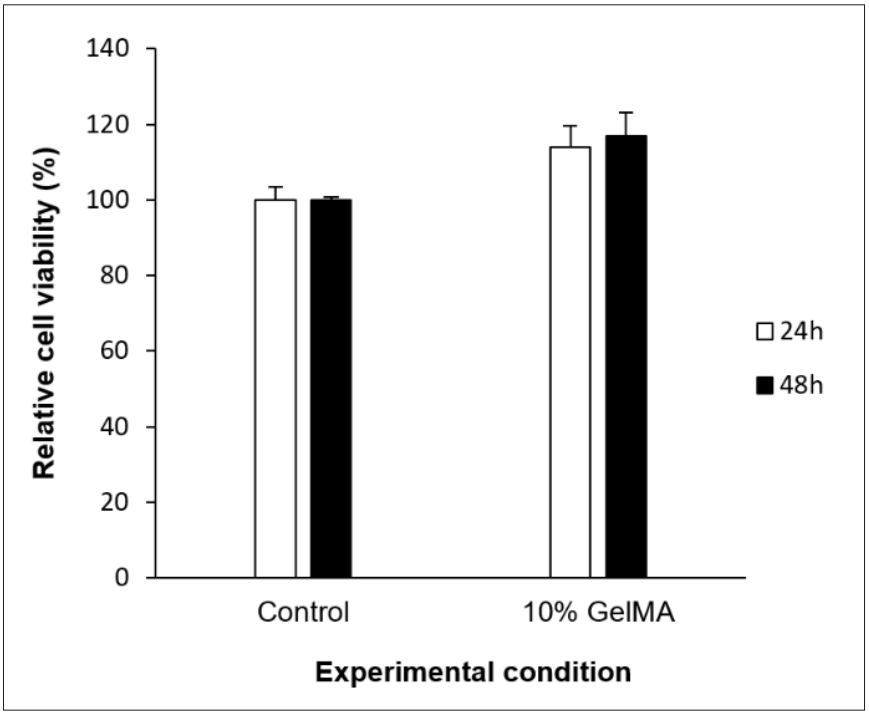

Figure 7. Cell viability of 10% gelatin methacryloyl (GelMA) relative to control after 24 and 48 hours (h) of growth. Data are presented as mean ± standard deviation of duplicate plates with triplicate conditions (n = 6).

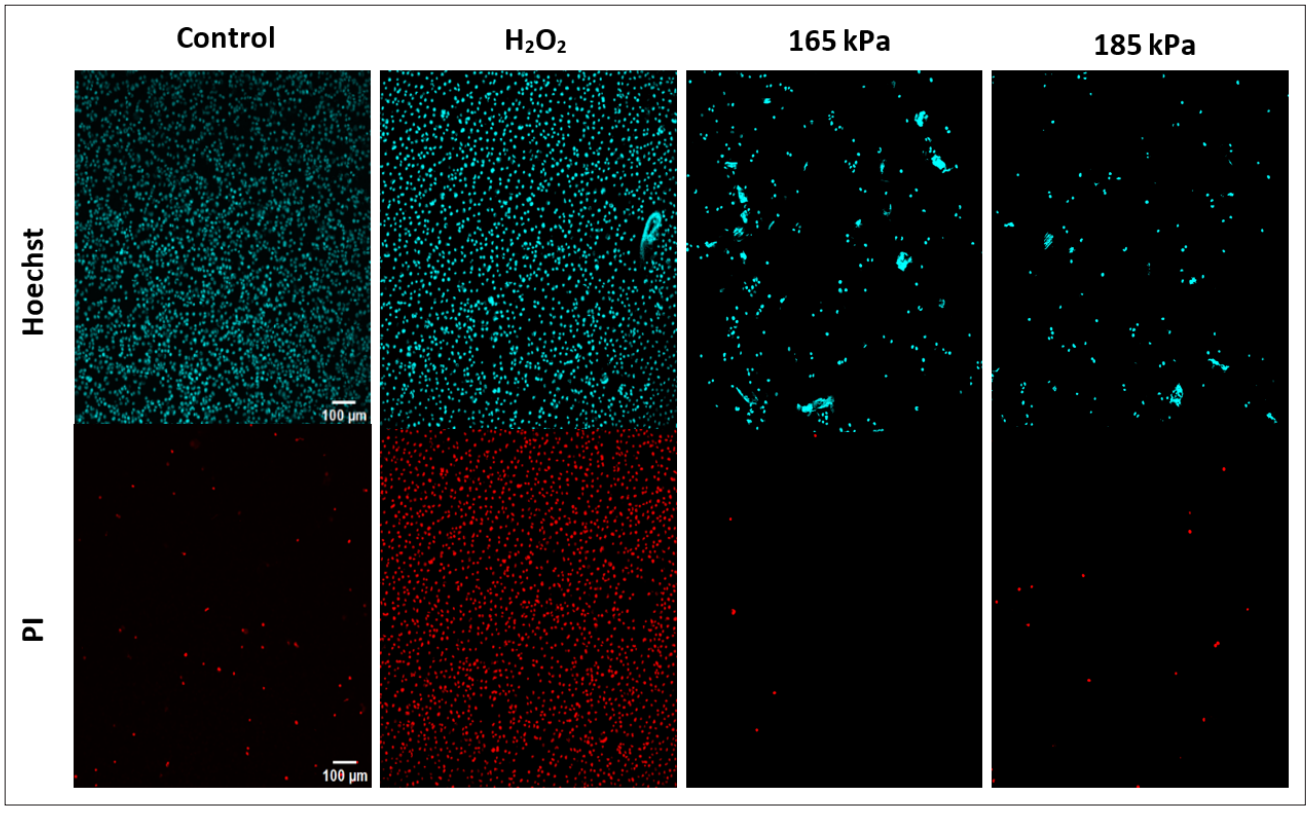

Figure 8. Phenotypic and apoptotic effects of pressure in 10% gelatin methacryloyl. Scale bar: 100 µm; magnification: 10×. Abbreviations: H_2O_2, hydrogen peroxide; PI, propidium iodide.

that acute mechanical stress during printing does not necessarily compromise longer-term cellular performance. For example, Zhao *et al.*[33] reported preserved cell viability up to 7 days after extrusion-based printing, while Ouyang *et al.*[41] demonstrated sustained survival and proliferation of embedded cells over extended culture periods in GelMA-based bioinks. These observations support the relevance of minimizing acute shear stress during printing.

4. Conclusion

This study presents an independent, modular characterization device designed to experimentally define extrusion pressure thresholds and stabilization ranges that can be transferred across extrusion-based bioprinting systems by enabling precise, real-time monitoring and quantitative characterization of extrusion pressure and hydrogel flow behavior. The system reliably identified both the minimum pressure required to initiate extrusion and the stabilization range in which continuous and uniform material flow was achieved. Operating within this pressure window reduced deposition variability and significantly enhanced the reproducibility and structural fidelity of printed constructs.

The conclusions of this work are supported by experimental validation, including force–displacement analysis, quantitative image-based assessment of printed structures, and biological evaluation. This approach aligns with recent studies showing that predictive models and off-line rheological characterization do not reliably describe the flow behavior of pseudoplastic hydrogels under extrusion-based bioprinting conditions, and that experimentally derived metrics are required to improve process reproducibility and interlaboratory comparability.

Analysis of hydrogel extrusion under different pressure conditions confirmed that extrusion pressure is a critical determinant of geometric accuracy. Sub-optimal pressures resulted in discontinuous or incomplete filaments, whereas excessive pressures caused filament swelling and loss of dimensional accuracy. In contrast, printing at the stabilization pressure produced homogeneous filaments, well-defined grids, and complex geometries with improved precision.

Biological validation further demonstrated that extrusion pressure directly influences post-printing cell survival. Pressures above the stabilization zone increased shear exposure and reduced viability, whereas optimal pressures preserved high survival rates. These findings highlight the dual importance of pressure optimization for both structural performance and biological integrity.

Compared with empirical trial-and-error calibration, the proposed device reduces material consumption, shortens optimization times, and enhances process reproducibility. Its modular configuration and compatibility with commercial bioprinters make it a versatile and practical tool for laboratories seeking quantitative and controllable extrusion conditions.

In summary, this device represents a relevant advancement for extrusion-based bioprinting by providing accurate measurement and control of key process parameters. Its implementation facilitates the fabrication of constructs with greater geometric fidelity and improved cell viability. This quantitative calibration strategy contributes to the standardization of extrusion bioprinting, reduces operator-dependent variability, and supports the reproducible generation of biologically meaningful structures for tissue engineering and advanced *in vitro* modeling.

Acknowledgments

The authors gratefully acknowledge the financial support of the European Union through the European Regional Development Fund (85%) and the Regional Government of Extremadura, managed by the Ministry of Finance, under project GR24001. The authors also acknowledge the support of the project BIOIMP_ACE_MAS_6_E (0140_BIOIMP_ACE_MAS_6_E), co-funded by the European Union through the Interreg VI-A Spain–Portugal Programme (POCTEP) 2021–2027 (2021TC16RFCB005) and the European Regional Development Fund (ERDF).

Funding

This research was co-financed (85%) by the European Union through the European Regional Development Fund and by the Regional Government of Extremadura. Managing Authority: Ministry of Finance, through project GR24001.This research was funded by the BIOIMP_ACE_MAS_6_E project (0140_BIOIMP_ACE_MAS_6_E), co-funded by the European Union through the Interreg VI-A Spain-Portugal Programme (POCTEP) 2021–2027 (2021TC16RFCB005) and the European Regional Development Fund (ERDF).

Conflict of interest

The authors declare that they have no conflicts of interest.

Author contributions

Conceptualization: Antonio Macías García and Silvia Díaz Prado.

Formal analysis: Alfonso Carlos Marcos Romero

Investigation: Laura Mendoza Cerezo and Jesús Manuel Rodríguez Rego
Methodology: Jesús Manuel Rodríguez Rego and Alfonso Carlos Marcos Romero
Writing – original draft: Antonio Macías García and Jesús Manuel Rodríguez Rego
Writing – review & editing: Silvia María Díaz Prado and Laura Mendoza Cerezo.

Ethics approval and consent to participate

Not applicable.

Consent for publication

Not applicable.

Availability of data

The authors confirm that the data supporting the findings of this study are available within the article.

References

1. Jiang T, Munguia-Lopez JG, Flores-Torres S, Kort-Mascort J, Kinsella JM. Extrusion bioprinting of soft materials: an emerging technique for biological model fabrication. *Appl Phys Rev*. 2019;6(1):011310. doi: 10.1063/1.5059393
2. Askari M, Afzali Naniz M, Kouhi M, Saberi A, Zolfagharian A, Bodaghi M. Recent progress in extrusion 3D bioprinting of hydrogel biomaterials for tissue regeneration: a comprehensive review with focus on advanced fabrication techniques. *Biomater Sci*. 2021;9(3): 535-573. doi: 10.1039/D0BM00973C
3. He C, He J, Wu C, *et al*. 3D printing for tissue/organ regeneration in China. *Bio Des Manuf*. 2025;8:169-244. doi: 10.1631/BDM.2400309
4. Murphy SV, Atala A. 3D bioprinting of tissues and organs. *Nat Biotechnol*. 2014;32(8):773-785. doi: 10.1038/nbt.2958
5. Ozbolat IT, Hospodiuk M. Current advances and future perspectives in extrusion-based bioprinting. *Biomaterials*. 2016;76:321-343. doi: 10.1016/J.BIOMATERIALS.2015.10.076
6. Geckil H, Xu F, Zhang X, Moon S, Demirci U. Engineering hydrogels as extracellular matrix mimics. *Nanomedicine (Lond)*. 2010;5(3):469-484. doi: 10.2217/NNM.10.12
7. Gopinathan J, Noh I. Recent trends in bioinks for 3D printing. *Biomater Res*. 2018;22(11):1-15. doi: 10.1186/S40824-018-0122-1
8. Wang H, Bi S, Shi B, *et al*. Recent advances in engineering bioinks for 3D bioprinting. *Adv Eng Mater*. 2023;25(19):2300648. doi: 10.1002/ADEM.202300648
9. Gasperini L, Mano JF, Reis RL. Natural polymers for the microencapsulation of cells. *J R Soc Interface*. 2014;11(100):20140817. doi: 10.1098/RSIF.2014.0817
10. Olabisi RM. Cell microencapsulation with synthetic polymers. *J Biomed Mater Res A*. 2015;103(2):846-859. doi: 10.1002/JBM.A.35205
11. Esfahani RR, Jun H, Rahmani S, Miller A, Lahann J. Microencapsulation of live cells in synthetic polymer capsules. *ACS Omega*. 2017;2(6):2839-2847. doi: 10.1021/acsomega.7b00570
12. Cardoso LM da F, Alves LA, Barreto T, Gama JFG. Natural biopolymers as additional tools for cell microencapsulation applied to cellular therapy. *Polymers*. 2022;14(13):2641. doi: 10.3390/POLYM14132641
13. Leberfinger AN, Ravnic DJ, Dhawan A, Ozbolat IT. Concise review: bioprinting of stem cells for transplantable tissue fabrication. *Stem Cells Transl Med*. 2017;6(10):1940. doi: 10.1002/SCTM.17-0148
14. Gu Q, Tomaskovic-Crook E, Lozano R, *et al*. Functional 3D neural mini-tissues from printed gel-based bioink and human neural stem cells. *Adv Healthc Mater*. 2016;5(12):1429-1438. doi: 10.1002/ADHM.201600095
15. Jeon O, Lee Y Bin, Jeong H, Lee SJ, Wells D, Alsberg E. Individual cell-only bioink and photocurable supporting medium for 3D printing and generation of engineered tissues with complex geometries. *Mater Horiz*. 2019;6(8):1625. doi: 10.1039/C9MH00375D
16. Boularaoui S, Al Hussein G, Khan KA, Christoforou N, Stefanini C. An overview of extrusion-based bioprinting with a focus on induced shear stress and its effect on cell viability. *Bioprinting*. 2020;20:e00093. doi: 10.1016/J.BPRINT.2020.E00093
17. Rossi A, Pescara T, Gambelli AM, *et al*. Biomaterials for extrusion-based bioprinting and biomedical applications. *Front Bioeng Biotechnol*. 2024;12:1393641. doi: 10.3389/fbioe.2024.1393641
18. Mirshafiei M, Rashedi H, Yazdian F, Rahdar A, Baino F. Advancements in tissue and organ 3D bioprinting: current techniques, applications, and future perspectives. *Mater Des*. 2024;240:112853. doi: 10.1016/J.MATDES.2024.112853
19. Jang J, Park JY, Gao G, Cho DW. Biomaterials-based 3D cell printing for next-generation therapeutics and diagnostics. *Biomaterials*. 2018;156:88-106.

doi: 10.1016/J.BIOMATERIALS.2017.11.030

20. Malda J, Visser J, Melchels FP, *et al*. 25th anniversary article: engineering hydrogels for biofabrication. *Adv Mater*. 2013;25(36):5011-5028.
doi: 10.1002/ADMA.201302042

21. Schwab A, Levato R, D'Este M, Piluso S, Eglin D, Malda J. Printability and shape fidelity of bioinks in 3D bioprinting. *Chem Rev*. 2020;120(19):11028-11055.
doi: 10.1021/ACS.CHEMREV.0C00084

22. Mendoza Cerezo L, Romero ACM, García AM, Amador JPC, Rego JMR. Recent advances in 3D bioprinting. *Compendium of 3D Bioprinting Technology*. Boca Raton: CRC Press; 2025:69-85.
doi: 10.1201/9781003505198-4

23. Rego JMR, Cendal AIR, Prado SMD, García AM, Romero ACM, Cerezo LM. 3D bioprinting of cartilage. *Compendium of 3D Bioprinting Technology*. Boca Raton: CRC Press; 2025:469-481.
doi: 10.1201/9781003505198-25

24. Datta P, Ayan B, Ozbolat IT. Bioprinting for vascular and vascularized tissue biofabrication. *Acta Biomater*. 2017;51:1-20.
doi: 10.1016/J.ACTBIO.2017.01.035

25. Strauß S, Schroth B, Hubbuch J. Evaluation of the reproducibility and robustness of extrusion-based bioprinting processes applying a flow sensor. *Front Bioeng Biotechnol*. 2022;10:831350.
doi: 10.3389/FBIOE.2022.831350/BIBTEX

26. Strauß S, Garces DG, Hubbuch J. Analytics in extrusion-based bioprinting: standardized methods improving quantification and comparability of the performance of bioinks. *Polymers*. 2023;15(8):1829.
doi: 10.3390/POLYM15081829

27. Grijalva Garces D, Strauß S, Gretzinger S, *et al*. On the reproducibility of extrusion-based bioprinting: round robin study on standardization in the field. *Biofabrication*. 2023;16(1):015002.
doi: 10.1088/1758-5090/ACFE3B

28. Armstrong AA, Pfeil A, Alleyne AG, Wagoner Johnson AJ. Process monitoring and control strategies in extrusion-based bioprinting to fabricate spatially graded structures. *Bioprinting*. 2021;21:e00126.
doi: 10.1016/J.BPRINT.2020.E00126

29. Mũnoz Z, Shih H, Lin CC. Gelatin hydrogels formed by orthogonal thiol–norbornene photochemistry for cell encapsulation. *Biomater Sci*. 2014;2(8):1063-1072.
doi: 10.1039/C4BM00070F

30. Eslahi N, Abdorahim M, Simchi A. Smart polymeric hydrogels for cartilage tissue engineering: a review on the chemistry and biological functions. *Biomacromolecules*. 2016;17(11):3441-3463.
doi: 10.1021/ACS.BIOMAC.6B01235

31. Xiao S, Zhao T, Wang J, *et al*. Gelatin methacrylate (GelMA)-based hydrogels for cell transplantation: an effective strategy for tissue engineering. *Stem Cell Rev Rep*. 2019;15(5):664-679.
doi: 10.1007/S12015-019-09893-4

32. Yue K, Trujillo-de Santiago G, Alvarez MM, Tamayol A, Annabi N, Khademhosseini A. Synthesis, properties, and biomedical applications of gelatin methacryloyl (GelMA) hydrogels. *Biomaterials*. 2015;73:254-271.
doi: 10.1016/J.BIOMATERIALS.2015.08.045

33. Zhao X, Lang Q, Yildirimer L, *et al*. Photocrosslinkable gelatin hydrogel for epidermal tissue engineering. *Adv Healthc Mater*. 2016;5(1):108-118.
doi: 10.1002/ADHM.201500005

34. Lee BH, Shirahama H, Cho NJ, Tan LP. Efficient and controllable synthesis of highly substituted gelatin methacrylamide for mechanically stiff hydrogels. *RSC Adv*. 2015;5(128):106094-106097.
doi: 10.1039/C5RA22028A

35. Sun M, Sun X, Wang Z, Guo S, Yu G, Yang H. Synthesis and properties of gelatin methacryloyl (GelMA) hydrogels and their recent applications in load-bearing tissue. *Polymers (Basel)*. 2018;10(11):1290.
doi: 10.3390/POLYM10111290

36. Arguchinskaya NV, Isaeva EV, Kisel AA, *et al*. Properties and printability of the synthesized hydrogel based on GelMA. *Int J Mol Sci*. 2023;24(3):2121.
doi: 10.3390/IJMS24032121

37. Han S, Kim CM, Jin S, Kim TY. Study of the process-induced cell damage in forced extrusion bioprinting. *Biofabrication*. 2021;13(3).
doi: 10.1088/1758-5090/AC0415

38. Paxton N, Smolan W, Böck T, Melchels F, Groll J, Jungst T. Proposal to assess printability of bioinks for extrusion-based bioprinting and evaluation of rheological properties governing bioprintability. *Biofabrication*. 2017;9(4):044107.
doi: 10.1088/1758-5090/AA8DD8

39. Ribeiro A, Blokzijl MM, Levato R, *et al*. Assessing bioink shape fidelity to aid material development in 3D bioprinting. *Biofabrication*. 2017;10(1):014102.
doi: 10.1088/1758-5090/AA90E2

40. Rodríguez-Rego JM, Mendoza-Cerezo L, Macías-García A, Carrasco-Amador JP, Marcos-Romero AC. Methodology for characterizing the printability of hydrogels. *Int J Bioprint*. 2023;9(2):280-291.
doi: 10.18063/IJB.V9I2.667

41. Ouyang L, Yao R, Zhao Y, Sun W. Effect of bioink properties on printability and cell viability for 3D bioplotting of embryonic stem cells. *Biofabrication*. 2016;8(3):035020.
doi: 10.1088/1758-5090/8/3/035020

42. Ángeles Pérez M, Compaired PM, García-Gareta E. An experimental workflow for bioprinting optimization:

application to a custom-made biomaterial ink. *Int J Bioprint*. 2025;11(3):397-415.
doi: 10.36922/IJB025120094

43. Naghieh S, Chen X. Printability–a key issue in extrusion-based bioprinting. *J Pharm Anal*. 2021;11(5):564-579.
doi: 10.1016/J.JPHA.2021.02.001

44. Malekpour A, Chen X. Printability and cell viability in extrusion-based bioprinting from experimental, computational, and machine learning views. *J Funct Biomater*. 2022;13(2):40.
doi: 10.3390/JFB13020040

45. Ning L, Betancourt N, Schreyer DJ, Chen X. Characterization of cell damage and proliferative ability during and after bioprinting. *ACS Biomater Sci Eng*. 2018;4(11): 3906-3918.
doi: 10.1021/acsbiomaterials.8b00714